

Rational Design of Ion Transport Paths at the Interface of Metal–Organic Framework Modified Solid Electrolyte

Yangyang Xia, Nuo Xu, Lulu Du, Yu Cheng, Shulai Lei, Shujuan Li, Xiaobin Liao, Wenchao Shi, Lin Xu,* and Liqiang Mai*



Cite This: *ACS Appl. Mater. Interfaces* 2020, 12, 22930–22938



Read Online

ACCESS |



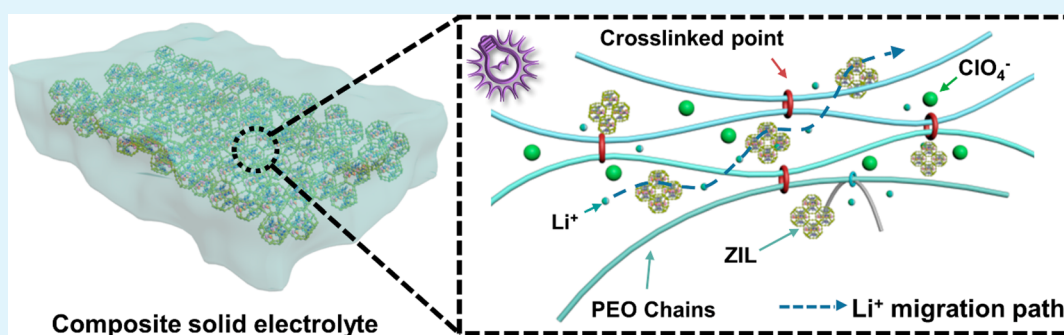
Metrics & More



Article Recommendations



Supporting Information



ABSTRACT: Solid-state lithium batteries have attracted great attention owing to their potential advantages in safety and energy density. Among various solid electrolytes, solid polymer electrolyte is promising due to its good viscoelasticity, lightweight, and low-cost processing. However, key issues of solid polymer electrolyte include poor ionic conductivity and low Li^+ transference number, which limit its practical application. Herein, a new-type of ultraviolet cross-linked composite solid electrolyte (C–CSE), composed of ZIF-based ionic conductor (named ZIL) and polymer, is designed with enhanced ion transport. The ZIL is composed of ZIF-8 and ionic liquid, which can provide C–CSE with fast ion transport paths. Moreover, the proper pore size of ZIF-8 can restrict the migration of embedded ionic liquid and thus construct a solid–liquid transport interface between polymer chains and ZIF-8, which could achieve fast ion transport. In addition, ultraviolet irradiation can decrease the crystallization of C–CSE and thus increase the amorphous region. Consequently, the C–CSE show excellent electrochemical performance including high ionic conductivity of 0.426 mS cm^{-1} at 30°C , high Li^+ transference number of 0.67, and good Li/Li compatibility cycle over 1040 h. Experimental and computational results indicate that diffusion energy barrier of Li^+ through ZIF-8 is smaller than that of polymer chains, which reveals a new Li^+ transport mechanism between polymer chains and ZIL, from “chain–chain–chain” to “chain–ZIL–chain”. This work demonstrates rational design of ion transport paths at the interface of solid electrolyte could facilitate the development of solid-state lithium batteries as a promising novel strategy.

KEYWORDS: ZIF-based ionic conductor, ultraviolet irradiation, interface design, lithium-ion transport mechanism, composite solid electrolyte

1. INTRODUCTION

Lithium-ion batteries (LIBs) have been widely applied in various fields such as portable electronics, electric automobile, and large-scale energy storage because of their high output power, low self-discharge, no memory effect, and environmental friendliness.¹ However, liquid organic electrolytes in commercial LIBs are vulnerable to generate side reactions during charging and discharging processes, which would result in irreversible fading of battery capacity.² Moreover, drawbacks of flammability and volatilization in liquid organic electrolytes are harmful to the safety and lifespan of batteries during service.^{3,4} Besides, commercial LIBs are mainly composed of graphite anode, failing to satisfy the growing demand for energy storage devices with high energy density.⁵ In contrast to

liquid organic electrolytes, solid-state electrolytes (SSEs) possess excellent performance, such as nonflammability, good electrochemical stability, and compatibility with lithium anode.^{6–8} This is why solid electrolyte is widely considered as the most promising next-generation technology to batteries.^{9–11} According to this, developing solid electrolytes

Received: March 7, 2020

Accepted: April 29, 2020

Published: April 29, 2020



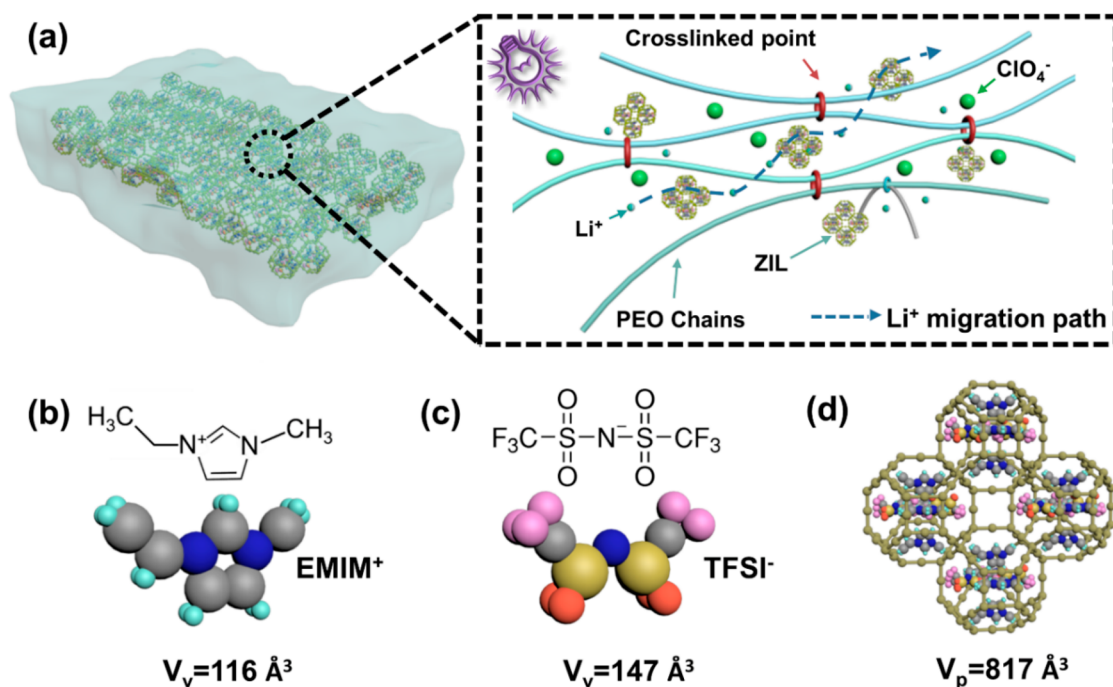


Figure 1. (a) Schematic illustration for the design of UV cross-linked composite solid electrolyte and Li⁺ migration path. (b) van der Waals volumes of EMIM⁺ (light blue sphere: H atom, black sphere: C atom, blue sphere: N atom). (c) van der Waals volumes of TFSI⁻ (purple sphere: F atom, black sphere: C atom, yellow sphere: S atom, blue sphere: N atom, orange sphere: O atom). (d) The structure of ZIF-based ionic conductor after incorporating (EMIM_{0.83}Li_{0.17})TFSI into ZIF-8 framework (V_p indicate pore volume of ZIF-8).

instead of liquid electrolytes has received wide attention in batteries with high safety and energy density.^{12,13}

SSEs are mainly divided into two categories: solid-state ceramic electrolytes and solid-state polymer electrolytes (SPEs).⁶ Nowadays, SPEs, such as poly(ethylene oxide) (PEO), have been generally considered as more promising solid electrolytes for commercialization because of their good flexibility, easy film formation, lightweight, low-cost processing, etc.¹⁴ Nevertheless, SPEs have also been hindered in practical application due to two key scientific issues of poor ionic conductivity and low lithium-ion mobility.^{15,16} In view of these challenges, numerous strategies have been developed to improve the performance of SPEs, such as copolymerization, blending, cross-linking, and complexing with inorganic particles.^{17–23} Recently, some solid ceramic/polymer composite electrolytes were reported that inorganic ceramic particles could considerably enhance ionic conductivity as active lithium-ion conductors by optimizing the interface of ion transport.^{24–27} Apart from this, cross-linked copolymer electrolytes were prepared and applied in energy storage devices, which proves the cross-linking effect in SPEs could enhance ion transport.^{28,29} Cross-linking of polymer can serve as a feasible and effective strategy on boosting the design of polymer networks, and hence obtaining the high performance electrolyte with great thermal stability and improved wettability of polymer matrix.^{30–33} Although these methods have been used to enhance the performance of solid electrolytes, it is still far from practical applications. Moreover, there have been few reports about SPEs with both high ionic conductivity and Li⁺ transference number. Thus, designing novel strategies, interfaces, and fillers to enhance ion transport in SSEs is of great significance in the development of high-performance SPEs.

Metal–organic frameworks (MOFs) show great prospects in electrolytes because they have low electrical conductivity and tunable pore structure.^{34,35} For example, MOF-modified liquid organic electrolyte has been reported to inhibit the dendrite growth of lithium.³⁶ Another significant finding is that a MOF-based electrolyte was designed by mixing UIO-67 and ionic liquid, which effectively improved the ion transport interface of Li₇La₃Zr₂O₁₂ in the Li₇La₃Zr₂O₁₂-based SSBs.³⁷ Unlike liquid organic electrolytes, ionic liquids (ILs) have advantages of nonflammability, higher ionic conductivity, wider electrochemical window and better electrodeposited lithium morphologies.^{38–43} Thereby, introducing ILs into MOFs can not only avoid the safety hazards from liquid organic electrolytes but also effectively improve ionic conductivity due to the desired interface of MOF-based electrolyte.³⁹ Besides, appropriate pore sizes of MOFs and Lewis acid–base interactions can limit the migration of cation/anion of ILs and release more free Li⁺ participating in ion transport, which have a positive influence on Li⁺ transference number.⁴⁴ On account of the above research, incorporating ILs into proper pores/channels of MOFs and the interface design between MOFs and composite materials are promising strategies to optimize ion transport in solid electrolytes.

In this work, a novel ultraviolet (UV) cross-linked composite solid electrolyte (C–CSE) based on ZIF-based ionic conductor (named ZIL) and PEO was designed and constructed. The ZIL is composed of ZIF-8, bis-(trifluoromethyl)sulfonylimide lithium salt (LiTFSI), and ionic liquid 1-ethyl-3-methylimidazolium-bis(trifluoromethylsulfonyl)imide (EMIM-TFSI). The porous ZIF-8 hosts serve as stable 3D frameworks to absorb (EMIM_{0.83}Li_{0.17})TFSI and limit the migration of EMIM⁺ and TFSI⁻, thus construct a solid–liquid transport interface between polymer chains and ZIF-8 in C–CSE. Based on the introducing of ZIL as the Li⁺

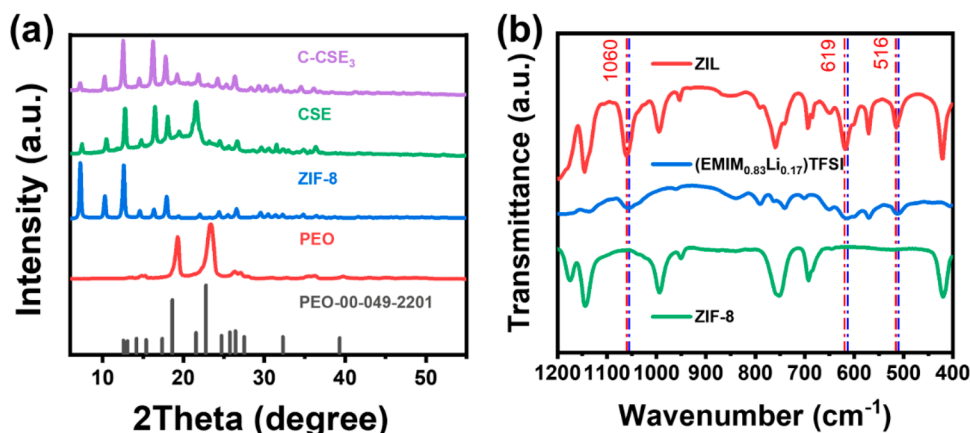


Figure 2. (a) XRD patterns of ZIF-8, PEO, CSE, and C-CSE₃. (b) FTIR spectra of ZIF-8, (EMIM_{0.83}Li_{0.17})TFSI and ZIL.

active filler, the inhibition effect of ZIF-8 micropores size on EMIM⁺, and Lewis acid–base interactions between the ZIF-8 host and anions, the ionic conductivity and Li⁺ transference number are enhanced. The UV irradiation can decrease the crystallization of polymer and thus increase the amorphous region, which can promote the fast and continuous ion transport. Moreover, the cross-linked polymer matrix can also restrict the migration of large-size anions and provide the C-CSE with excellent electrochemical and mechanical stability. Meanwhile, we proposed a unique Li⁺ transport mechanism on the solid–liquid transport interface of polymer chains and ZIL from “chain–chain–chain” to “chain-ZIL-chain”. Owing to the superior structure and effective Li⁺ transport, the obtained electrolyte exhibited a high ionic conductivity of 0.426 mS cm⁻¹ and high Li⁺ transference number of 0.67 ± 0.08. Besides, it also exhibited a wide potential window and excellent lithium metal compatibility.

2. EXPERIMENTAL SECTION

2.1. Preparation of the ZIL. The ZIF-8 was prepared via a mild solution stirring method.⁴⁵ The experimental drugs were purchased from Aladdin without further treatment. First, 1 mmol of zinc nitrate hexahydrate [Zn(NO₃)₂·6 H₂O] and 8 mmol of 2-methylimidazole (C₄H₆N₂) were added in 14 mL of methanol, respectively. Then, the mixture was stirred and mixed for 24 h. Second, ZIF-8 was obtained by centrifugal washing with methanol. By heating the ZIF-8 at 120 °C for 12 h, the activated ZIF-8 can be obtained. Third, based on the concentration of lithium salt and the relationship between viscosity of ionic liquid and ionic conductivity, the (EMIM_{0.83}Li_{0.17})TFSI was prepared by mixing 2.5 mmol of LiTFSI and 5 g of (EMIM)TFSI through magnetic stirring (the molar ratio of EMIM⁺: Li⁺ was 5:1).^{46,47} A different amount of (EMIM_{0.83}Li_{0.17})TFSI was added to the activated ZIF-8, separately. Finally, the mixing materials of activated ZIF-8 and (EMIM_{0.83}Li_{0.17})TFSI were heated at 120 °C in an oven for 12 h to obtain ZIF-based ionic conductor.

2.2. Preparation of C-CSE. The related drugs were purchased from Aladdin without further treatment. First, LiClO₄ was grinded by ball milling to obtain the smaller particle of LiClO₄ at a rotate speed of 250 r/min for 24 h. Then PEO (MW = 600 000), LiClO₄, and ZIL were mixed and grinded in an agate mortar by ball milling. Then, a mold (the diameter is 17 mm) was used to obtain the CSE membrane at 20 MPa by hot pressing. Cross-linked fluid was composed of LiTFSI (1M), 4-methylbenzophenone (MBP; 0.5 M), and tetraethylene-glycol-dimethyl-ether (TEGDME; 2.2 mmol). Then 10 μL of cross-linked fluid was added in CSE, and that was evenly distributed into CSE after 12 h. Finally, ultraviolet irradiation was executed to acquire C-CSE by cross-linking the CSE membrane in 10 min. After that, the C-CSE was placed in a glovebox for 1 day

before further characterization and testing. The detailed characterization, electrochemical measurement, and theoretical calculations are shown in the [Supporting Information](#).

3. RESULTS AND DISCUSSION

3.1. Morphology and Structure Characterization of Solid Electrolyte.

The C-CSE was prepared by UV irradiation combined with hot pressing. The structure and components of C-CSE are illustrated in [Figure 1a](#), including PEO chain, ZIL and LiClO₄, where the blue dotted line is denoted as the Li⁺ migration path between ZIL and PEO chains in the as-obtained C-CSE. ZIL ([Figure 1d](#)) composed of ZIF-8 and (EMIM_{0.83}Li_{0.17})TFSI was prepared by thermal mixing, encapsulating the (EMIM_{0.83}Li_{0.17})TFSI component in the ZIF-8 framework. The (EMIM_{0.83}Li_{0.17})TFSI was selected as Li⁺ conductive guest, where EMIM⁺ is the 1-ethyl-3-methylimidazolium cation ([Figure 1b](#)) and TFSI⁻ is the bis(trifluoromethylsulfonyl)amide anion ([Figure 1c](#)).⁴⁸ ZIF-8 crystals have a pore volume of 0.663 cm³ g⁻¹ and the 3D framework with the sodalite topology constructed from the Zn²⁺ and MeIm⁻ ligands (a large apertures of 11.6 Å and a small pores of 3.4 Å).^{45,49} ZIF-8 was chosen to be the host of (EMIM_{0.83}Li_{0.17})TFSI due to its high porosity, proper pore size, and chemical stability. The micropore size of ZIF-8 can limit the migration of EMIM⁺ (7.6 Å of length and 4.3 Å of width) and TFSI⁻ (7.9 Å of length and 2.6 Å of width).⁵⁰ What's more, based on the Lewis acid–base theory, TFSI⁻ is a Lewis base, while the Zn²⁺ in nanosized ZIF-8 behaves as a Lewis acid, offering ZIF-8 the feature to restrain the TFSI⁻ from moving in ZIL and releasing more free Li⁺ to participate in the ion transport.⁵¹ The cross-linked PEO matrix was synthesized by using the PEO as polymer chain, MBP as the photo initiator (the light-induced hydrogen abstraction mediator), and tetraglyme molecule including dissolved MBP as the active plasticizer via UV irradiation. In the process of UV irradiation, MBP abstracts acidic protons from –CH₂– (methylene groups) in PEO and creates a free radical with active domain. Then, numerous free radical could combine other free radical from the identical molecule chain or other PEO segments to form a cross-linked polymer. Moreover, tetraglyme could also form oligomers, or link to the neighboring PEO segments by the same hydrogen abstraction from methylene groups in tetraglyme. So the whole cross-linked processing included the realignment of PEO segments, the cross-linking of PEO and tetraglyme, and the oligomerization of tetraglyme.^{52,53} Finally, the ultraviolet cross-linked PEO

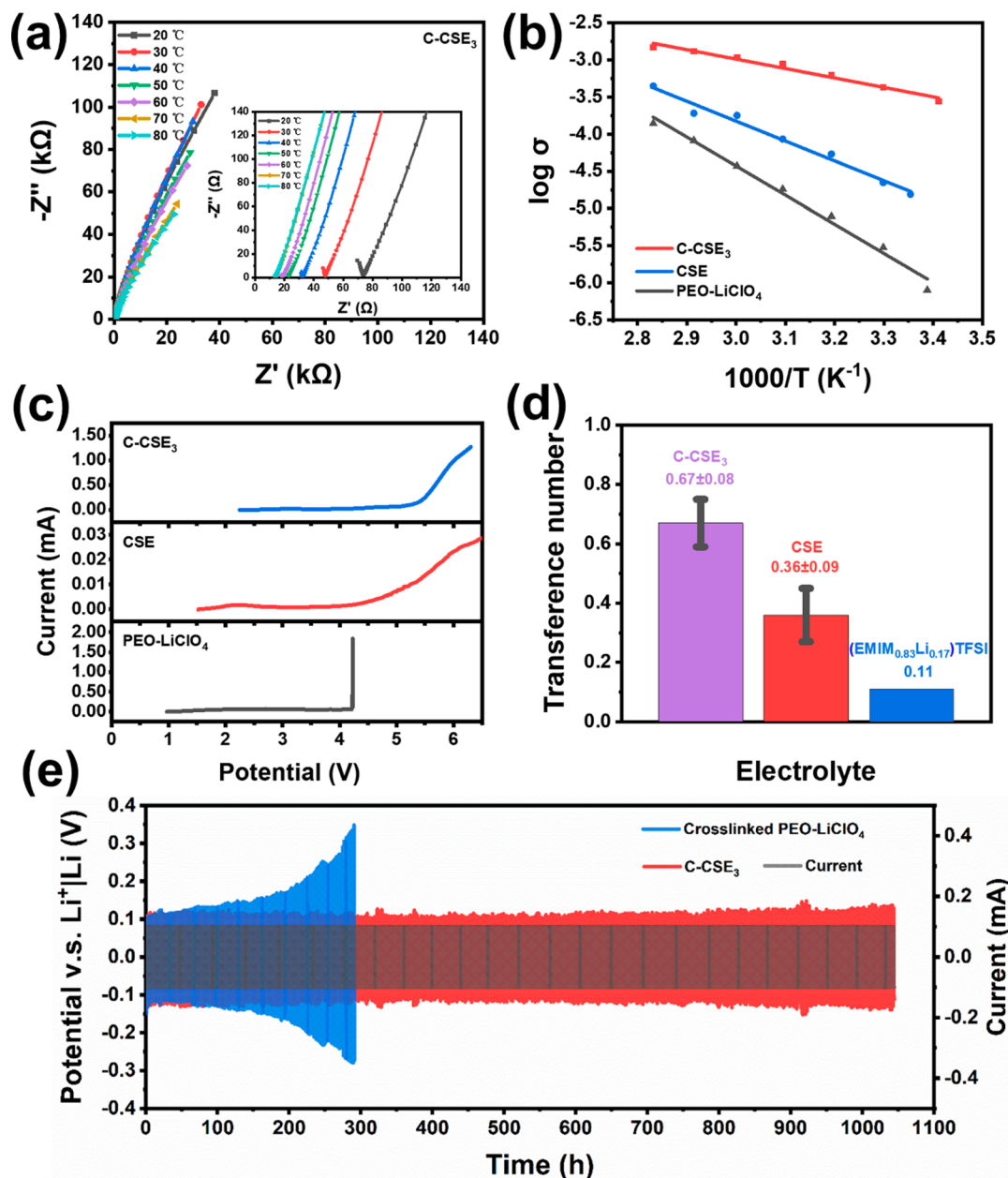


Figure 3. (a) EIS of UV cross-linked electrolyte (C-CSE₃) within frequency of 0.1 Hz–1 MHz at temperature from 20 to 80 °C, inset: magnified high frequency region. (b) Arrhenius plots of C-CSE₃, CSE, and PEO-LiClO₄. (c) Electrochemical windows of C-CSE₃, CSE, and PEO-LiClO₄ with a scan speed of 5 mV s⁻¹ at 25 °C. (d) Li⁺ transference number of C-CSE₃ and CSE. (e) Lithium compatibility cycling of lithium|C-CSE₃|lithium and lithium|cross-linked PEO-LiClO₄|lithium symmetrical cells.

matrix is mainly amorphous and possesses the good flexibility and mechanical strength because of the interpenetrating architecture and the generation of oligomers.

Scanning electron microscopy (SEM) image of ZIF-8 is shown in Figure S1a. The diameter of ZIF-8 can be observed from transmission electron microscope (TEM), which is calculated to be about 25 nm (Figure S1b). Figure S2 exhibits the X-ray diffraction (XRD) pattern of ZIF-8, and the peaks located in 011, 002, and 112 are coincident with those in the reported literature, indicating the successful synthesis of ZIF-8.⁵⁸ After introducing the (EMIM)_{0.83}Li_{0.17}TFSI into ZIF-8, homogeneous ZIL is shown in SEM image (Figure S1c), which is free of cracks and possesses a smoother surface compared with ZIF-8. In order to explore the effect of ZIL components and UV irradiation on solid electrolytes, different samples were

prepared, like C-CSE₁ (wt. 20% of ZIL with UV irradiation; Figure S3a), C-CSE₂ (wt. 40% of ZIL with UV irradiation; Figure S3b), C-CSE₃ (wt. 60% of ZIL with UV irradiation; Figure S3c) and C-CSE₄ (wt. 80% of ZIL with UV irradiation; Figure S3d), CSE (wt. 60% of ZIL without UV irradiation; Figure S3e). All samples of SEM images show the solid electrolyte has good miscibility and homogeneity. Further evidence of the energy dispersive spectrometer of C-CSE₃ is displayed in Figure S4. The uniform distribution of elements C, O, Zn, Cl, and S demonstrates that PEO, ZIF-8, LiClO₄, and TFSI⁻ have good miscibility. In C-CSE₃, the interaction of Lewis acid sites in ZIF-8 and Lewis base centers in PEO chains could promote the dissociation of metal salts and decrease the crystallinity in PEO by reducing ionic coupling.⁵⁴

Thus, ZIF-8 as the framework of ZIL can improve the miscibility of the C–CSE₃.

XRD patterns of ZIF-8, PEO, CSE, and C–CSE₃ are displayed in Figure 2a, proving the decreased crystallinity of the polymer in the presence of ZIL and after UV irradiation. As is shown in the pattern, the PEO shows the sharp peaks of crystallization. After adding ZIL into PEO, the intensity of peaks decreases to some extent. Just like ceramic particles, the ZIF-8 in nanosized ZIL has Lewis acid sites, while the polymer PEO possesses Lewis base centers, based on the Lewis acid–base theory, the interaction in the nanocomposite electrolyte result in reduced crystallinity in PEO.⁵⁴ After the UV irradiation, the interpenetrative architecture, the disordered network, and oligomers were formed by the UV-derived cross-linking reaction; thus, UV irradiation can decrease the crystallization of PEO.⁵³ The XRD results demonstrate that both ZIL components and UV cross-linking can reduce the crystallinity of C–CSE₃ and increase the proportion of amorphous region. Besides, XRD patterns of C–CSE₁, C–CSE₂, C–CSE₃, and C–CSE₄ are shown in Figure S3f. With the increasing amount of ZIL, the crystallization intensity of peaks weakens and the width of PEO peaks decreases, implying the lower crystallization in C–CSE₃. For PEO-based SSEs, the lower crystallinity can lead to high ionic conductivity and facilitate lithium-ion transport between PEO chains, because lithium-ion adsorption and transport mainly occur in amorphous regions.⁵⁵

In order to investigate the interaction of (EMIM_{0.83}Li_{0.17})-TFSI and ZIF-8 framework, XRD, nitrogen gas adsorption, and FTIR were tested at room temperature. (EMIM_{0.83}Li_{0.17})-TFSI was incorporated into ZIF-8 framework to obtain the ZIL with different mass ratio [ZIF-8: (EMIM_{0.83}Li_{0.17})-TFSI = 1:1 and ZIF-8: (EMIM_{0.83}Li_{0.17})-TFSI = 1:1.5], where (EMIM_{0.83}Li_{0.17})-TFSI theoretically occupied the different micropores volume of the ZIF-8 framework. These mixtures were transferred into an oven and then stored for 12 h to enhance the diffusion of (EMIM_{0.83}Li_{0.17})-TFSI in micropores of ZIF-8 framework. XRD patterns of ZIL and ZIF-8 (Figure S2) show that the structure of ZIF-8 remained stable even after mixing with (EMIM_{0.83}Li_{0.17})-TFSI and subsequent heating. With the increasing of (EMIM_{0.83}Li_{0.17})-TFSI mass fraction, the peak intensity of 011 decreased while 013 increased (Figure S2). These results indicate the change of electron density in micropores of ZIF-8 after incorporating the (EMIM_{0.83}Li_{0.17})-TFSI into ZIF-8 framework.^{38,48} In addition, the Type-I adsorption is observed in nitrogen gas adsorption (Figure S5).⁵⁶ The pore volume (0.666 cm³ g⁻¹) of ZIF-8 was tested by Brunauer–Emmett–Teller (BET), which is consistent with the literature.⁴⁵ After adding 0.665 mL of (EMIM_{0.83}Li_{0.17})-TFSI into ZIF-8, the pore volume of this ZIF-8 framework is reduced by 100%, and this agrees with the theoretical calculated value. The result shows the pore volume of ZIF-8 framework is filled of (EMIM_{0.83}Li_{0.17})-TFSI. Besides, FTIR spectra of (EMIM_{0.83}Li_{0.17})-TFSI, ZIF-8 and ZIL are shown in Figure 2b. These marked peaks at 1060, 619, and 516 cm⁻¹ (red dot dash line) in ZIL should belong to the (EMIM_{0.83}Li_{0.17})-TFSI (blue dot dash line).³⁵ The blue shift from (EMIM_{0.83}Li_{0.17})-TFSI can be explained by the disaggregation of ion pairs, because ions enter in ZIF-8 micropores, which indicates ZIL possesses a more stable structure after introducing the (EMIM_{0.83}Li_{0.17})-TFSI into ZIF-8.³⁸ There is limited space to accommodate less than three ion pairs in each micropore of ZIF-8, which can be confirmed by using the van

der Waals volumes of EMIM⁺ and TFSI⁻.⁵⁷ Based on the XRD, BET, and FTIR, these results demonstrate that (EMIM_{0.83}Li_{0.17})-TFSI can be successfully incorporated in micropores of framework without destroying the structure of ZIF-8.

3.2. Electrochemical Performance of Solid Electrolyte. In view of the pore volume of ZIF-8, the mass ratio of ZIF-8: (EMIM_{0.83}Li_{0.17})-TFSI = 1:1, was selected in the electrochemical characterizations. The C–CSE was assembled into a closed battery and used the model of stainless steel/solid electrolyte/stainless steel for the measurement of electrochemical impedance spectroscopy (EIS). The EIS results of C–CSE₃ (Figure 3a), CSE (Figure S6a), and PEO–LiClO₄ (Figure S6b) were tested in frequency from 0.1 Hz to 1 M Hz at the temperature from 20 to 80 °C. The C–CSE₃ shows the minimum bulk resistance (48 Ω) compared with the CSE (716 Ω) and PEO–LiClO₄ (11633 Ω) at 30 °C. The ionic conductivities of C–CSE₃, CSE, and PEO–LiClO₄ were 4.26 × 10⁻⁴, 2.22 × 10⁻⁵, and 2.99 × 10⁻⁶ S cm⁻¹ at 30 °C, respectively, which was calculated by eq S1. The Arrhenius plots of the C–CSE₃, CSE, and PEO–LiClO₄ can be acquired according to ionic conductivity and are shown in Figure 3b. The corresponding activation energies (E_a) of lithium-ion transport are 0.25, 0.53, and 0.77 eV, respectively. Meanwhile, the Arrhenius plots of C–CSE₁, C–CSE₂, and C–CSE₄ are demonstrated in Figure S7, and the detailed data comparison of ionic conductivity and E_a are shown in Table S1. These display that C–CSE₃ have the highest ionic conductivity and the lowest E_a. With the increase of ZIL components, the ionic conductivity rise up because more ZIL provide faster Li⁺ transport paths in contrast with PEO in C–CSE₃. While ZIL components increase to 80%, the ionic conductivity is lower on account of a discontinuous Li⁺ pathway of independent ZIL particles. Less PEO chains in C–CSE₄ was insufficient to afford the interparticle ion transport because PEO chains can provide the lithium-ion transport at the gap between ZIF-8 in solid electrolytes. Thus, the C–CSE₃ has an effective ion transport based on the optimal dosage of ZIL components and UV crosslinked PEO. In addition, the cross-linked PEO matrix can provide the C–CSE₃ with mechanical stability, because it can realize stronger support compared with the individual ZIL particle.

The electrochemical stability of solid electrolyte was tested by linear sweep voltammetry (LSV). The electrochemical window ranging from open-circuit voltage to 6.5 V is presented to investigate the electrochemical stability of solid electrolytes (Figure 3c). The electrochemical window of pristine PEO–LiClO₄ is 4.2 V, expanding to 4.5 V with ZIL as fillers, with the help of UV irradiation, ending up with an increase to 5.2 V. The above results prove that combining ZIL and UV cross-linking can significantly provide positive synergies to improve the electrochemical stability of solid electrolytes, offering a potential application of high-voltage cathode materials and high energy density batteries.

The Evans method was used to measure the Li⁺ transference number (*t*_{Li⁺}) of solid electrolytes in lithium/solid electrolyte/lithium symmetric battery by applying a constant polarization potential of 10 mV at 25 °C (eq S2).⁵⁸ Figure S8 shows the polarization curve of C–CSE₃ at the potential of 10 mV at 25 °C and the inset is EIS of lithium|C–CSE₃|lithium symmetric battery before and after polarization. The comparison of *t*_{Li⁺} for different electrolyte materials were shown in Figure 3d in order to study ion transport. The *t*_{Li⁺} of C–CSE₃, CSE and

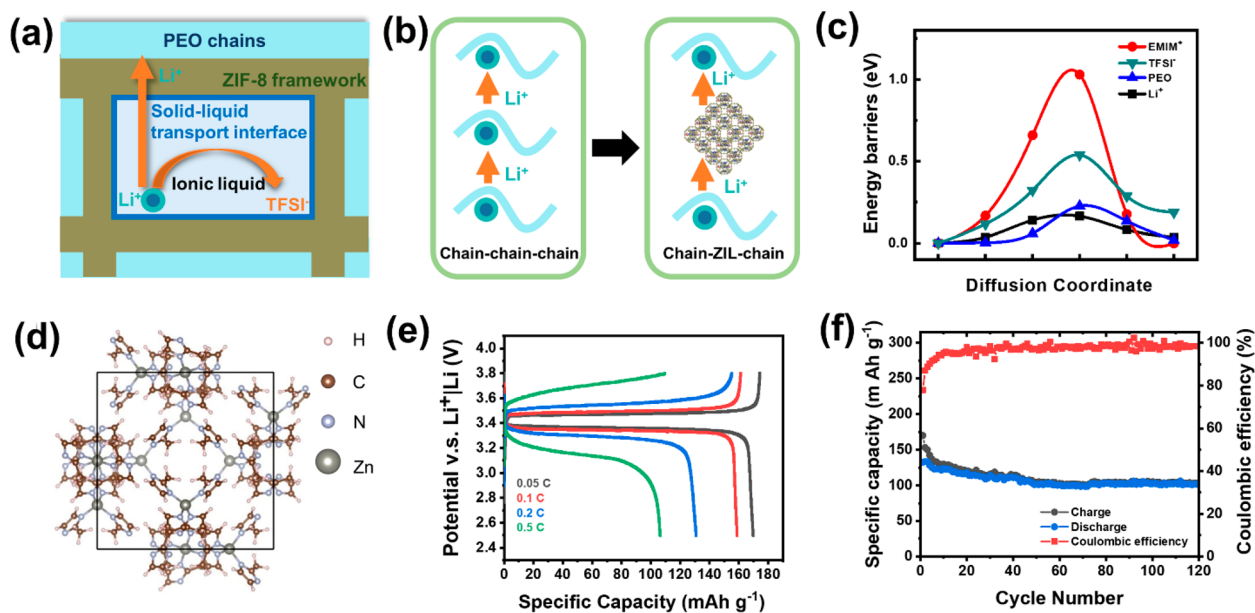


Figure 4. (a) Schematic illustration for the Li⁺ transport mechanism on a solid–liquid transport interface. (b) The new-model Li⁺ transport mechanism from “chain–chain–chain” to “chain-ZIL-chain”. (c) Diffusion energy barrier of EMIM⁺, TFSI⁻, and Li⁺ through ZIF-8 (blue color: diffusion energy barrier of Li⁺ between PEO chains). (d) Optimized configuration of ZIF-8, in which pink, brown, light-blue, and gray colors are for H, C, N, and Zn atoms, respectively. (e) The charge and discharge performance of LiFePO₄|C–CSE₃ lithium batteries at different current rate of 0.05, 0.1, 0.2, and 0.5 C. (f) Cycling performance and Coulombic efficiency of the LiFePO₄|C–CSE₃ lithium battery at a 0.1 C charge/discharge rate.

(EMIM_{0.83}Li_{0.17})TFSI is 0.67 ± 0.08 , 0.36 ± 0.09 and 0.11, respectively.³⁷ The pristine (EMIM_{0.83}Li_{0.17})TFSI electrolyte shows a low t_{Li^+} contributed from the EMIM⁺ and TFSI⁻ rather than Li⁺.⁴⁰ When mixing ZIL, PEO, and LiClO₄, the t_{Li^+} of CSE is 0.36 ± 0.09 . While combining the ZIL and UV irradiation, the C–CSE₃ shows the highest t_{Li^+} (0.67 ± 0.08). The ZIF-8 as scaffold can not only limit the migration of EMIM⁺ because of the embedded EMIM⁺ into micropores of ZIF-8, but also immobilize anions by Lewis acid–base interactions, which helps to release more free Li⁺ to participate in the ion transport. The result shows that the cross-linked PEO matrix and ZIL can enhance t_{Li^+} by the inhibition effect of ZIF-8 micropores on EMIM⁺, Lewis acid–base interactions between the ZIF-8 hosts and anions, and the restriction of cross-linked polymer matrix on anions.^{50,59}

The lithium compatibility test of C–CSE₃ was executed with a current of 0.1 mA at 25 °C and the result is shown in Figure 3e. The polarization potential of the symmetric battery is 100 mV, which is sustained of 2 h for each full cycle of charging and discharging process. No short circuit is observed and the polarization potential is consistent (red curve) over 1040 h. The detailed cycling of lithium compatibility is shown in Figure S9. The result demonstrates the adding of ZIL components can provide stable interface between C–CSE₃ and lithium metal. This may be attributed to uniform dispersal of ZIL in the PEO matrix, which can construct a symmetrical and efficient ion transport network on the interface between C–CSE₃ and lithium metal to prevent the growth of lithium dendrites.^{44,60} As a contrast, the cross-linked PEO–LiClO₄ without ZIL was prepared, and the voltage of the symmetric cell extends to 300 mV after cycling 300 h (blue curve), which implies an unstable Li⁺ transport on the interface.

3.3. Li⁺ Transport Mechanism and Batteries Performance of Solid Electrolyte. For the purpose of the analysis of the Li⁺ transport mechanism, EIS plots of solid electrolytes

were studied. C–CSE₃ possesses the highest ionic conductivity and lowest bulk resistance due to the synergies of ZIL and UV irradiation, which can be proved by the smaller semicircle of its EIS plot in Figure 3a compared with CSE (Figure S6a) and PEO–LiClO₄ (Figure S6b). In C–CSE₃, the polymer chains are entirely filled with nanosized ZIL particles, which can act as highways for the Li⁺ transport between polymer chains. In addition, the uniformly dispersed ZIL particles in C–CSE₃ can make direct contact with polymer chains through open channels of ZIF-8 framework (Figure 4a). In PEO-based SPEs, the migration of Li⁺ is achieved by the segmental motion of polymer by the complexation and decomplexation of lithium ions and etheroxy groups.⁶¹ While in C–CSE₃, lithium ions at the surface of polymer chains are first solvated by TFSI⁻, and then go into ZIL where equal amount of lithium ions are desolvated and transported to other PEO chains.⁶² The whole interfacial process seems like a solid–liquid transport interface, facilitating the Li⁺ transport in C–CSE₃. Such a “solid–liquid transport interface” mechanism is schematically illustrated in Figure 4a and the new-model Li⁺ transportation from “chain–chain–chain” to “chain-ZIL-chain” is shown in Figure 4b. Thus, the solid–liquid transport interface between polymer and ZIL is actually wetted by (EMIM_{0.83}Li_{0.17})TFSI at the atomic scale and beneficial to the effective Li⁺ transport. In order to demonstrate the Li⁺ transport in solid electrolytes, the delayed first transmission (DFT) was used to study the diffusion energy barrier of Li⁺ in this electrolyte (Figure 4c,d). The DFT results show that the diffusion energy barrier of Li⁺ through ZIF-8 is smaller than EMIM⁺ and TFSI⁻, even smaller than that of PEO chains, which demonstrates that the Li⁺ transport can be enhanced after introducing the ZIF-8 into polymer chains. This conforms to the lowest E_a and highest t_{Li^+} of C–CSE₃. Furthermore, oxygen atoms in TFSI⁻ and hydrogen atoms in ZIF-8 are easily formed into hydrogen bonds, providing the ZIL with a more stable structure (Figure

4d), which is coincident with the blue shift in Figure 2b. It is reasonable that UV cross-linked polymer chains will change this configuration to depress TFSI⁻ diffusion, realizing higher t_{Li^+} .

In order to explore the potential application of solid electrolytes, batteries of LiFePO₄|C–CSE₃|Li were assembled and tested. The discharge capacities of 167, 160, 130, and 105 mA h g⁻¹ are obtained and the low polarization voltages at around 0.105, 0.153, 0.247, and 0.431 V under the different current density of 0.05, 0.1, 0.2, and 0.5 C (1 C = 155 mA g⁻¹), respectively (Figure 4e). The low potential polarization and well-defined potential plateau at different current densities demonstrate that the electrode and solid electrolyte possess the superior conductivity, structural integrity, and good reversible cycling process, which was corresponding to the typical two-phase behavior of the cathode material (Fe²⁺/Fe³⁺ reversible redox reaction).^{11,26} Besides, the assembled batteries show good cycling performance with capacity retention of 76.8% beyond 120 cycles, and the capacity degradation is calculated to be about 0.19% for every cycle (Figure 4f). In terms of the Coulombic efficiency, it is 78% in the first cycle of batteries, and then increases to about 95% after 10 cycles. The performance of different types of MOF-based electrolytes is listed in Table S2, which aimed to compare the C–CSE₃ with other reported works. The findings suggest that the obtained C–CSE₃ have excellent comprehensive performance including ionic conductivity and t_{Li^+} based on the superior structure, effective Li⁺ transport, and a unique solid–liquid transport interface mechanism. All of the results demonstrate that the C–CSE₃ can be used as a promising solid electrolyte to apply in the field of lithium batteries.

4. CONCLUSIONS

In summary, a novel composite solid electrolyte was obtained by using a ZIF-based ionic conductor as filler combined with UV irradiation. The ZIF-8 host existed in the ZIF-based ionic conductor as a porous 3D framework has the ability to establish direct interface contact between inner solidified (EMIM_{0.83}Li_{0.17})TFSI and polymer chains, providing the electrolyte with a high selectivity of Li⁺ transport. The UV irradiation can decrease the crystallization of the polymer thus increasing the amorphous region, which can promote the continuous ion transport and increase ionic conductivity. Hence, the C–CSE₃ demonstrates the expanding potential window (vs Li/Li⁺; >5.2 V), higher ionic conductivity (0.426 mS cm⁻¹), high t_{Li^+} (0.67 ± 0.08), and excellent compatibility with lithium metal over 1040 h. Finally, the new-model Li⁺ transport mechanism on the solid–liquid transport interface, which is between polymer chains and ZIL from “chain–chain–chain” to “chain–ZIL–chain”, is demonstrated according to the experimental and computational results of Li⁺ diffusion energy barrier. All of the results suggest that this work contributes to the increase of ionic conductivity and t_{Li^+} of SPEs, which will shed light on the design of efficient solid electrolytes with enhanced ion transport by rational design of the interface.

■ ASSOCIATED CONTENT

Supporting Information

The Supporting Information is available free of charge at <https://pubs.acs.org/doi/10.1021/acsami.0c04387>.

Additional experimental details including Figures S1–S9 and Tables 1 and 2 (PDF)

■ AUTHOR INFORMATION

Corresponding Authors

Liqiang Mai – State Key Laboratory of Advanced Technology for Materials Synthesis and Processing, International School of Materials Science and Engineering, Wuhan University of Technology, Wuhan 430070, China; Foshan Xianhu Laboratory of the Advanced Energy Science and Technology Guangdong Laboratory, Foshan 528200, China; orcid.org/0000-0003-4259-7725; Email: mlq518@whut.edu.cn

Lin Xu – State Key Laboratory of Advanced Technology for Materials Synthesis and Processing, International School of Materials Science and Engineering, Wuhan University of Technology, Wuhan 430070, China; Foshan Xianhu Laboratory of the Advanced Energy Science and Technology Guangdong Laboratory, Foshan 528200, China; orcid.org/0000-0003-2347-288X; Email: linxu@whut.edu.cn

Authors

Yangyang Xia – State Key Laboratory of Advanced Technology for Materials Synthesis and Processing, International School of Materials Science and Engineering, Wuhan University of Technology, Wuhan 430070, China

Nuo Xu – State Key Laboratory of Advanced Technology for Materials Synthesis and Processing, International School of Materials Science and Engineering, Wuhan University of Technology, Wuhan 430070, China

Lulu Du – State Key Laboratory of Advanced Technology for Materials Synthesis and Processing, International School of Materials Science and Engineering, Wuhan University of Technology, Wuhan 430070, China

Yu Cheng – State Key Laboratory of Advanced Technology for Materials Synthesis and Processing, International School of Materials Science and Engineering, Wuhan University of Technology, Wuhan 430070, China

Shulai Lei – Hubei Key Laboratory of Low Dimensional Optoelectronic Materials and Devices, Hubei University of Arts and Science, Xiangyang 441053, China

Shujuan Li – Hubei Key Laboratory of Low Dimensional Optoelectronic Materials and Devices, Hubei University of Arts and Science, Xiangyang 441053, China

Xiaobin Liao – State Key Laboratory of Advanced Technology for Materials Synthesis and Processing, International School of Materials Science and Engineering, Wuhan University of Technology, Wuhan 430070, China

Wenchao Shi – State Key Laboratory of Advanced Technology for Materials Synthesis and Processing, International School of Materials Science and Engineering, Wuhan University of Technology, Wuhan 430070, China

Complete contact information is available at: <https://pubs.acs.org/doi/10.1021/acsami.0c04387>

Author Contributions

L.M. and L.X. were in charge of this scientific research project, and the leaders of actual coordination of contributions. Y.X. performed all of the experiments and the data analyses as well as wrote the manuscript. N.X., L.D., and Y.C. contributed to the conception of the study and revised the manuscript. S.L. and S.L. performed the density functional theory calculations. X.L. and W.S. helped discuss and revise the manuscript.

Notes

The authors declare no competing financial interest.

ACKNOWLEDGMENTS

This work was supported by the National Natural Science Foundation of China (51802239), Foshan Xianhu Laboratory of the Advanced Energy Science and Technology Guangdong Laboratory (XHT2020-005 and XHT2020-003), the Natural Science Foundation of Hubei Province (2019CFA001), the Fundamental Research Funds for the Central Universities (2019IVB054 and 2019III062JL), and the Hubei University of Arts and Science (XK2019052).

REFERENCES

- (1) Armand, M.; Tarascon, J. M. Building better batteries. *Nature* **2008**, *451*, 652–657.
- (2) Yu, K.; Pan, X.; Zhang, G.; Liao, X.; Zhou, X.; Yan, M.; Xu, L.; Mai, L. Nanowires in Energy Storage Devices: Structures, Synthesis, and Applications. *Adv. Energy Mater.* **2018**, *8*, 1802369.
- (3) Mauger, A.; Armand, M.; Julien, C. M.; Zaghbi, K. Challenges and issues facing lithium metal for solid-state rechargeable batteries. *J. Power Sources* **2017**, *353*, 333–342.
- (4) Xie, D.; Zhang, M.; Wu, Y.; Xiang, L.; Tang, Y. A Flexible Dual-Ion Battery Based on Sodium-Ion Quasi-Solid-State Electrolyte with Long Cycling Life. *Adv. Funct. Mater.* **2020**, *30*, 1906770.
- (5) Fan, L.; Wei, S.; Li, S.; Li, Q.; Lu, Y. Recent Progress of the Solid-State Electrolytes for High-Energy Metal-Based Batteries. *Adv. Energy Mater.* **2018**, *8*, 1702657.
- (6) Manthiram, A.; Yu, X.; Wang, S. Lithium battery chemistries enabled by solid-state electrolytes. *Nat. Rev. Mater.* **2017**, *2* (4), 16103.
- (7) Zheng, H.; Wu, S.; Tian, R.; Xu, Z.; Zhu, H.; Duan, H.; Liu, H. Intrinsic Lithiophilicity of Li-Garnet Electrolytes Enabling High-Rate Lithium Cycling. *Adv. Funct. Mater.* **2020**, *30*, 1906189.
- (8) Wang, C.; Yang, Y.; Liu, X.; Zhong, H.; Xu, H.; Xu, Z.; Shao, H.; Ding, F. Suppression of Lithium Dendrite Formation by Using LAGP-PEO (LiTFSI) Composite Solid Electrolyte and Lithium Metal Anode Modified by PEO (LiTFSI) in All-Solid-State Lithium Batteries. *ACS Appl. Mater. Interfaces* **2017**, *9* (15), 13694–13702.
- (9) Hao, X.; Zhu, J.; Jiang, X.; Wu, H.; Qiao, J.; Sun, W.; Wang, Z.; Sun, K. Ultrastrong Polyoxazole Nanofiber Membranes for Dendrite-Proof and Heat-Resistant Battery Separators. *Nano Lett.* **2016**, *16*, 2981–2987.
- (10) Xie, M.; Lin, X.; Huang, Z.; Li, Y.; Zhong, Y.; Cheng, Z.; Yuan, L.; Shen, Y.; Lu, X.; Zhai, T.; Huang, Y. A Li-Al-O Solid-State Electrolyte with High Ionic Conductivity and Good Capability to Protect Li Anode. *Adv. Funct. Mater.* **2020**, *30*, 1905949.
- (11) Yao, Y.; Wei, Z.; Wang, H.; Huang, H.; Jiang, Y.; Wu, X.; Yao, X.; Wu, Z. S.; Yu, Y. Toward High Energy Density All Solid-State Sodium Batteries with Excellent Flexibility. *Adv. Energy Mater.* **2020**, *10*, 1903698.
- (12) Everts, E. C. To the limits of lithium. *Nature* **2015**, *526*, S93–S95.
- (13) Tang, W.; Tang, S.; Guan, X.; Zhang, X.; Xiang, Q.; Luo, J. High-Performance Solid Polymer Electrolytes Filled with Vertically Aligned 2D Materials. *Adv. Funct. Mater.* **2019**, *29*, 1900648.
- (14) Zhang, J.; Yang, J.; Dong, T.; Zhang, M.; Chai, J.; Dong, S.; Wu, T.; Zhou, X.; Cui, G. Aliphatic Polycarbonate-Based Solid-State Polymer Electrolytes for Advanced Lithium Batteries: Advances and Perspective. *Small* **2018**, *14*, 1800821.
- (15) Xu, L.; Tang, S.; Cheng, Y.; Wang, K.; Liang, J.; Liu, C.; Cao, Y.-C.; Wei, F.; Mai, L. Interfaces in Solid-State Lithium Batteries. *Joule* **2018**, *2*, 1991–2015.
- (16) Lv, F.; Wang, Z.; Shi, L.; Zhu, J.; Edström, K.; Mindemark, J.; Yuan, S. Challenges and development of composite solid-state electrolytes for high-performance lithium ion batteries. *J. Power Sources* **2019**, *441*, 227175.
- (17) Zhang, J.; Yue, L.; Hu, P.; Liu, Z.; Qin, B.; Zhang, B.; Wang, Q.; Ding, G.; Zhang, C.; Zhou, X.; Yao, J.; Cui, G.; Chen, L. Taichi-inspired rigid-flexible coupling cellulose-supported solid polymer electrolyte for high-performance lithium batteries. *Sci. Rep.* **2015**, *4*, 6272.
- (18) Young, N. P.; Devaux, D.; Khurana, R.; Coates, G. W.; Balsara, N. P. Investigating polypropylene-poly(ethylene oxide)-polypropylene triblock copolymers as solid polymer electrolytes for lithium batteries. *Solid State Ionics* **2014**, *263*, 87–94.
- (19) Nguyen, H.-D.; Kim, G.-T.; Shi, J.; Paillard, E.; Judeinstein, P.; Lyonnard, S.; Bresser, D.; Iojoiu, C. Nanostructured multi-block copolymer single-ion conductors for safer high-performance lithium batteries. *Energy Environ. Sci.* **2018**, *11* (11), 3298–3309.
- (20) Lin, D.; Liu, W.; Liu, Y.; Lee, H. R.; Hsu, P. C.; Liu, K.; Cui, Y. High Ionic Conductivity of Composite Solid Polymer Electrolyte via In Situ Synthesis of Monodispersed SiO₂ Nanospheres in Poly(ethylene oxide). *Nano Lett.* **2016**, *16* (1), 459–465.
- (21) Li, Y.; Sun, Z.; Liu, D.; Gao, Y.; Wang, Y.; Bu, H.; Li, M.; Zhang, Y.; Gao, G.; Ding, S. A composite solid polymer electrolyte incorporating MnO₂ nanosheets with reinforced mechanical properties and electrochemical stability for lithium metal batteries. *J. Mater. Chem. A* **2020**, *8* (4), 2021–2032.
- (22) Zhang, J.; Zang, X.; Wen, H.; Dong, T.; Chai, J.; Li, Y.; Chen, B.; Zhao, J.; Dong, S.; Ma, J.; Yue, L.; Liu, Z.; Guo, X.; Cui, G.; Chen, L. High-voltage and free-standing poly(propylene carbonate)/Li_{6.75}La₃Zr_{1.75}Ta_{0.25}O₁₂ composite solid electrolyte for wide temperature range and flexible solid lithium ion battery. *J. Mater. Chem. A* **2017**, *5* (10), 4940–4948.
- (23) Li, D.; Chen, L.; Wang, T.; Fan, L. Z. 3D Fiber-Network-Reinforced Bicontinuous Composite Solid Electrolyte for Dendrite-free Lithium Metal Batteries. *ACS Appl. Mater. Interfaces* **2018**, *10* (8), 7069–7078.
- (24) Fu, K. K.; Gong, Y.; Dai, J.; Gong, A.; Han, X.; Yao, Y.; Wang, C.; Wang, Y.; Chen, Y.; Yan, C.; Li, Y.; Wachsmann, E. D.; Hu, L. Flexible, solid-state, ion-conducting membrane with 3D garnet nanofiber networks for lithium batteries. *Proc. Natl. Acad. Sci. U. S. A.* **2016**, *113* (26), 7094–7099.
- (25) Bae, J.; Li, Y.; Zhang, J.; Zhou, X.; Zhao, F.; Shi, Y.; Goodenough, J. B.; Yu, G. A 3D Nanostructured Hydrogel-Framework-Derived High-Performance Composite Polymer Lithium-Ion Electrolyte. *Angew. Chem., Int. Ed.* **2018**, *57*, 2096–2100.
- (26) Chen, L.; Li, Y.; Li, S.-P.; Fan, L.-Z.; Nan, C.-W.; Goodenough, J. B. PEO/garnet composite electrolytes for solid-state lithium batteries: From “ceramic-in-polymer” to “polymer-in-ceramic”. *Nano Energy* **2018**, *46*, 176–184.
- (27) Liu, L.; Qi, X.; Yin, S.; Zhang, Q.; Liu, X.; Suo, L.; Li, H.; Chen, L.; Hu, Y.-S. In Situ Formation of a Stable Interface in Solid-State Batteries. *ACS Energy Letters* **2019**, *4* (7), 1650–1657.
- (28) Chen, S.; Wang, J.; Wei, Z.; Zhang, Z.; Deng, Y.; Yao, X.; Xu, X. One-pot synthesis of crosslinked polymer electrolyte beyond 5V oxidation potential for all-solid-state lithium battery. *J. Power Sources* **2019**, *431*, 1–7.
- (29) Siyal, S. H.; Li, M.; Li, H.; Lan, J.-L.; Yu, Y.; Yang, X. Ultraviolet irradiated PEO/LATP composite gel polymer electrolytes for lithium-metallic batteries (LMBs). *Appl. Surf. Sci.* **2019**, *494*, 1119–1126.
- (30) Oh, B.; Il Jung, W.; Kim, D. W.; Rhee, H. W. Preparation of UV Curable Gel Polymer Electrolytes and Their Electrochemical Properties. *Bull. Korean Chem. Soc.* **2002**, *23*, 683–687.
- (31) Kim, S.-H.; Choi, K.-H.; Cho, S.-J.; Park, J.-S.; Cho, K. Y.; Lee, C. K.; Lee, S. B.; Shim, J. K.; Lee, S.-Y. A shape-deformable and thermally stable solid-state electrolyte based on a plastic crystal composite polymer electrolyte for flexible/safer lithium-ion batteries. *J. Mater. Chem. A* **2014**, *2*, 10854–10861.
- (32) Na, W.; Lee, A. S.; Lee, J. H.; Hwang, S. S.; Kim, E.; Hong, S. M.; Koo, C. M. Lithium Dendrite Suppression with UV-Curable Polysilsesquioxane Separator Binders. *ACS Appl. Mater. Interfaces* **2016**, *8*, 12852–12858.
- (33) Kil, E. H.; Choi, K. H.; Ha, H. J.; Xu, S.; Rogers, J. A.; Kim, M. R.; Lee, Y. G.; Kim, K. M.; Cho, K. Y.; Lee, S. Y. Polymer Electrolytes: Imprintable, Bendable, and Shape-Conformable Polymer Electrolytes

for Versatile-Shaped Lithium-Ion Batteries. *Adv. Mater.* **2013**, *25*, 1395–1400.

(34) Zhao, R.; Liang, Z.; Zou, R.; Xu, Q. Metal-Organic Frameworks for Batteries. *Joule* **2018**, *2* (11), 2235–2259.

(35) Chen, N.; Li, Y.; Dai, Y.; Qu, W.; Xing, Y.; Ye, Y.; Wen, Z.; Guo, C.; Wu, F.; Chen, R. A Li⁺ conductive metal organic framework electrolyte boosts the high-temperature performance of dendrite-free lithium batteries. *J. Mater. Chem. A* **2019**, *7* (16), 9530–9536.

(36) Bai, S.; Sun, Y.; Yi, J.; He, Y.; Qiao, Y.; Zhou, H. High-Power Li-Metal Anode Enabled by Metal-Organic Framework Modified Electrolyte. *Joule* **2018**, *2* (10), 2117–2132.

(37) Wang, Z.; Wang, Z.; Yang, L.; Wang, H.; Song, Y.; Han, L.; Yang, K.; Hu, J.; Chen, H.; Pan, F. Boosting interfacial Li⁺ transport with a MOF-based ionic conductor for solid-state batteries. *Nano Energy* **2018**, *49*, 580–587.

(38) Fujie, K.; Yamada, T.; Ikeda, R.; Kitagawa, H. Introduction of an ionic liquid into the micropores of a metal-organic framework and its anomalous phase behavior. *Angew. Chem., Int. Ed.* **2014**, *53* (42), 11302–11305.

(39) Watanabe, M.; Thomas, M.; Zhang, S.; Ueno, K.; Yasuda, T.; Dokko, K. Application of Ionic Liquids to Energy Storage and Conversion Materials and Devices. *Chem. Rev.* **2017**, *117*, 7190–7293.

(40) Galiński, M.; Lewandowski, A.; Stępnik, I. Ionic liquids as electrolytes. *Electrochim. Acta* **2006**, *51* (26), 5567–5580.

(41) Cheng, Y.; Zhang, L.; Xu, S.; Zhang, H.; Ren, B.; Li, T.; Zhang, S. Ionic liquid functionalized electrospun gel polymer electrolyte for use in a high-performance lithium metal battery. *J. Mater. Chem. A* **2018**, *6* (38), 18479–18487.

(42) Chen, R.; Qu, W.; Qian, J.; Chen, N.; Dai, Y.; Guo, C.; Huang, Y.; Li, L.; Wu, F. Zirconia-supported solid-state electrolytes for high-safety lithium secondary batteries in a wide temperature range. *J. Mater. Chem. A* **2017**, *5* (47), 24677–24685.

(43) Liu, H.; Yu, H. Ionic liquids for electrochemical energy storage devices applications. *J. Mater. Sci. Technol.* **2019**, *35* (4), 674–686.

(44) Liu, W.; Mi, Y.; Weng, Z.; Zhong, Y.; Wu, Z.; Wang, H. Functional metal-organic framework boosting lithium metal anode performance via chemical interactions. *Chem. Sci.* **2017**, *8* (6), 4285–4291.

(45) Park, K. S.; Ni, Z.; Cote, A. P.; Choi, J. Y.; Huang, R.; Uribe-Romo, F. J.; Chae, H. K.; O’Keeffe, M.; Yaghi, O. M. Exceptional chemical and thermal stability of zeolitic imidazolate frameworks. *Proc. Natl. Acad. Sci. U. S. A.* **2006**, *103* (27), 10186–10191.

(46) Garcia, B.; Lavallée, S.; Perron, G.; Michot, C.; Armand, M. Room temperature molten salts as lithium battery electrolyte. *Electrochim. Acta* **2004**, *49* (26), 4583–4588.

(47) Lassegues, J. C.; Grondin, J.; Talaga, D. Lithium solvation in bis(trifluoromethanesulfonyl)imide-based ionic liquids. *Phys. Chem. Chem. Phys.* **2006**, *8* (48), 5629–5632.

(48) Fujie, K.; Ikeda, R.; Otsubo, K.; Yamada, T.; Kitagawa, H. Lithium Ion Diffusion in a Metal–Organic Framework Mediated by an Ionic Liquid. *Chem. Mater.* **2015**, *27* (21), 7355–7361.

(49) Moh, P. Y.; Cubillas, P.; Anderson, M. W.; Attfield, M. P. Revelation of the Molecular Assembly of the Nanoporous Metal Organic Framework ZIF-8. *J. Am. Chem. Soc.* **2011**, *133* (34), 13304–13307.

(50) Largeot, C.; Portet, C.; Chmiola, J.; Taberna, P.-L.; Gogotsi, Y.; Simon, P. Relation between the Ion Size and Pore Size for an Electric Double-Layer Capacitor. *J. Am. Chem. Soc.* **2008**, *130*, 2730–2731.

(51) Chen, J.; Huang, L.; Wang, Q.; Wu, W.; Zhang, H.; Fang, Y.; Dong, S. Bio-inspired nanozyme: a hydratase mimic in a zeolitic imidazolate framework. *Nanoscale* **2019**, *11* (13), 5960–5966.

(52) Porcarelli, L.; Gerbaldi, C.; Bella, F.; Nair, J. R. Super Soft All-Ethylene Oxide Polymer Electrolyte for Safe All-Solid Lithium Batteries. *Sci. Rep.* **2016**, *6*, 19892.

(53) Zhang, Y.; Lu, W.; Cong, L.; Liu, J.; Sun, L.; Mauger, A.; Julien, C. M.; Xie, H.; Liu, J. Cross-linking network based on Poly(ethylene oxide): Solid polymer electrolyte for room temperature lithium battery. *J. Power Sources* **2019**, *420*, 63–72.

(54) Reddy, M. J.; Chu, P. P.; Kumar, J. S.; Rao, U. V. S. Inhibited crystallization and its effect on conductivity in a nano-sized Fe oxide composite PEO solid electrolyte. *J. Power Sources* **2006**, *161* (1), 535–540.

(55) Das, D.; Chandrasekaran, A.; Venkatram, S.; Ramprasad, R. Effect of Crystallinity on Li Adsorption in Polyethylene Oxide. *Chem. Mater.* **2018**, *30*, 8804–8810.

(56) SING, K. S. W. Reporting physisorption data for gas/solid. *Pure Appl. Chem.* **1982**, *54*, 2201–2218.

(57) Ue, M.; Murakami, A.; Nakamura, S. Convenient Method to Estimate Ion Size for Electrolyte Materials Design. *J. Electrochem. Soc.* **2002**, *149* (10), 1385–1388.

(58) Evans, J.; Vincent, C. A.; Bruce, P. G. Electrochemical measurement of transference numbers in polymer electrolytes. *Polymer* **1987**, *28* (13), 2324–2328.

(59) Choi, H.; Kim, H. W.; Ki, J.-K.; Lim, Y. J.; Kim, Y.; Ahn, J.-H. Nanocomposite quasi-solid-state electrolyte for high-safety lithium batteries. *Nano Res.* **2017**, *10* (9), 3092–3102.

(60) Tan, G.; Wu, F.; Zhan, C.; Wang, J.; Mu, D.; Lu, J.; Amine, K. Solid-State Li-Ion Batteries Using Fast, Stable, Glassy Nanocomposite Electrolytes for Good Safety and Long Cycle-Life. *Nano Lett.* **2016**, *16* (3), 1960–1968.

(61) Wright, P. V. Polymer electrolytes—the early days. *Electrochim. Acta* **1998**, *43*, 1137–1143.

(62) Lesch, V.; Heuer, A.; Tatsis, V. A.; Holm, C.; Smiatek, J. Peptides in the presence of aqueous ionic liquids: tunable co-solutes as denaturants or protectants? *Phys. Chem. Chem. Phys.* **2015**, *17* (39), 26049–26053.